Strength and stiffness parameters of Albany silica sand

Lohani, Tara Nidhi
Kawamata, Yohsuke
Tani, Kazuo
Iizuka, Atsushi
Kawai, Katsuyuki

(Citation)
神戸大学都市安全研究センター研究報告,25:297-307

(Issue Date)
2021-03

(Resource Type)
departmental bulletin paper

(Version)
Version of Record

(JaLCDOI)
https://doi.org/10.24546/81013303

(URL)
https://hdl.handle.net/20.500.14094/81013303

神戸大学都市安全研究センター
研究報告，第25号，令和３年３月

Strength and stiffness parameters of Albany silica sand

Tara Nidhi Lohani[1)]
Yohsuke Kawamata[2)]
Kazuo Tani[3)]
Atsushi Iizuka[4)]
Katsuyuki Kawai[5)]

Abstract: Mechanical strength parameters of the Albany silica sand were assessed by performing monotonic drained and undrained triaxial compression tests in the laboratory. Shear modulus at a very small strain (G_{max}) and its variation with strain, as demanded by many numerical models, were evaluated by recording the data at a very small strain level with the help of local deformation gauges. The stiffness data were further corroborated from the laboratory bender element (BE) tests that are widely adopted in geotechnical laboratories.

Keywords: Triaxial test, Albany sand, Local Deformation transducer, Bender element

1. INTRODUCTION

A highly dilatant Albany silica sand from Australia is being used in various research purposes in Japan (Kawamata et. al., 2016, MEXT and NIED, 2006, 2007). As mineral composition, grain-size distribution and frictional characteristics of sand particles from one origin produces a typical behavior that may differ with the samples from other origin, a comprehensive test plan was drawn in this research to conduct several series of drained and undrained triaxial tests by using Albany sand in the laboratory and evaluate strength, stiffness behavior experimentally. The stiffness at very small strain was obtained by attaching local deformation transducers (LDTs) to the cylindrical test specimens. In addition, the maximum initial shear modulus of the tested sand at a very small strain ($G_{\max}$) were also evaluated from shear wave velocity measured by a set of bender elements (BE) mounted on the triaxial testing apparatus (JGS-TC29, 2005; Lohani et.al, 1999).

2. MATERIAL AND TESTING DEVICE

(1) Test Material

Gradation curve of Albany silica sand #48 under this study is shown in Fig. 1. The well-graded and sub-angular-shaped silica sand particles mostly fall under medium to fine sand. Fines fraction is almost absent.

On comparing with the Toyoura sand, a widely used sand in Japan (Fukushima and Tatsuoka, 1984; Cubrinovski and Ishihara, 2002), both the maximum (e_{max}) and minimum (e_{min}) void ratio values (e_{max} =0.98, e_{min} =0.63 for Toyoura sand) as well as the void ratio range (e_{max}-e_{min}) are considerably smaller.

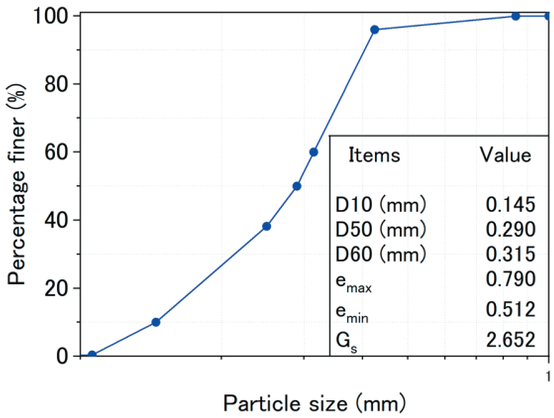

Fig.1. Grain size distribution of Albany sand.

(2) Testing Apparatus

In the triaxial testing system used for the test, a direct drive motor pushes the triaxial cell with specimen upwards and the load cell fixed externally with the piston at the top measures the applied load. A linear variable differential transformer (LVDT) attached externally measured an external strain. In triaxial cell used for Series II tests, a transmitter bender element (BE) and a receiver BE were fitted in the top cap and the bottom pedestal, respectively for measuring the shear wave velocity. A control software prepared at the laboratory has maintained the required back pressure, cell pressure and the loading speed automatically and with a very high accuracy.

3. TRIAXIAL TESTING PROCESS

(1) Specimen preparation

Air-pluviation method was applied to prepare the specimens. Air-dried sand was dropped into the specimen mold that was fitted with 0.2mm thick rubber membrane through a funnel on the top. In order to prepare the specimens with their target density, aperture size of the funnel and drop height were adjusted for each test series. Table 1 summarizes the prepared density and void ratio of test specimens.

(2) Preparing for small strain measurement

In order to measure the deformations at very small strain range, local deformation transducers (LDTs) (Goto et. al., 1991) were attached to the cylindrical test specimens in Series II tests. The sensor setup around the specimens are explained with the photograph and a schematic drawing is given in Fig. 2. Hinges were fixed with glue at the designated locations on rubber membrane and LDTs were attached. The longitudinal strain was measured by two LDTs in longitudinal direction, which were set at diametrically opposite sides. For lateral strain measurement, two semi-circular LDTs were attached to the specimen at 1/3rd and 2/3rd height by means of hinges located at diametrically opposite side (Fig. 2b). The change in specimen diameter measured by these two gauges were averaged to calculate the average lateral strain at any stage.

(3) Test Plan

Two series of consolidated drained (CD) test and one series of consolidated undrained tests with pore pressure measurements ($\overline{CU}$) were planned in order to understand the overall picture of strength behavior of

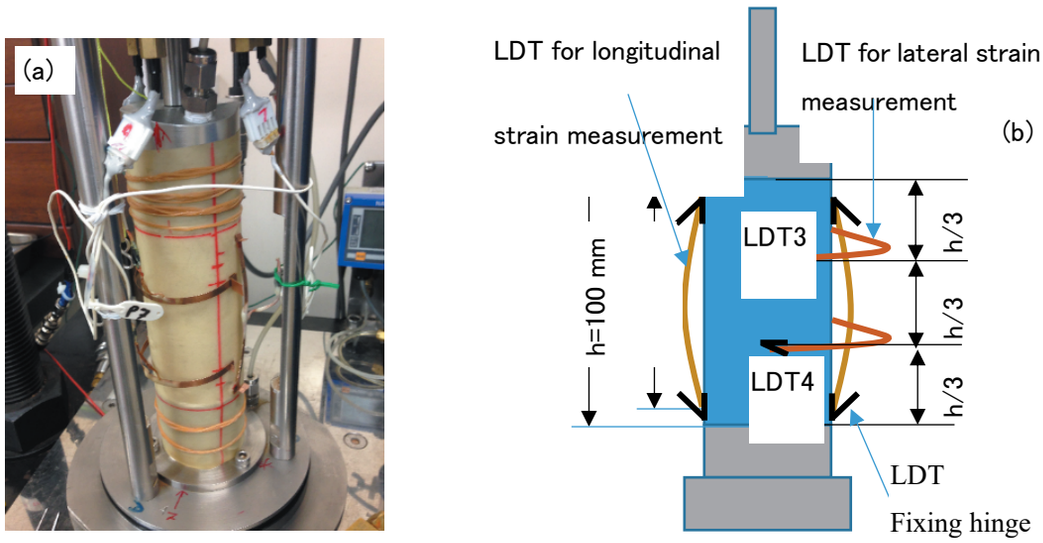

Fig. 2. a) Specimen fitted with local deformation transducers (LDT), and b) schematic diagram for LDT attachments to the specimen

this typical sand. Although desirable for all series, BE and LDT measurements were only done in Series II. Specimen prepared and their test conditions are summarized in Table 1. In general, axial stress and strain measurements were respectively taken with load cell and deformation gauges placed outside of the triaxial cell. Saturation was achieved by double vacuum method (JGS 2534, 2009) and applying back pressure (B.P.) of 200 kPa.

Table 1. Summary of testing conditions

Series	Test Type	Confining stress σ_c' (kPa)	D_r prepared (%)	Initial dry density (g/cm^3)	Initial void ratio	Shear strain rate (%/min)
I	$\overline{CU}$ (B.P. = 200 kPa)	100	81.0	1.710	0.551	0.02
		200	79.1	1.735	0.529	
		400	81.3	1.721	0.541	
II	CD with BE and LDTs (B.P.=200 kPa)	100	69.4	1.663	0.589	0.10
		200	69.8	1.668	0.582	
		400	71.2	1.664	0.578	
III	CD (B.P. = 200 kPa)	100	85.5	1.711	0.541	0.10
		200	83.2	1.703	0.546	
		400	77.6	1.687	0.551	

In addition to Table 1, the other details for each series are described in the following paragraphs.

Series I) $\overline{CU}$ tests: Pore water pressure was measured at the bottom end of dense specimens (Dr≈80%) of this series. Expecting a significant negative pore water pressure generation, a very low strain rate of 0.02 %/min was applied for sample shearing. This rate is considerably smaller than 0.05 to 0.1 %/min range recommended in JGS 0523 (2009) for ordinary silty- or sandy-soils.

Series II) CD tests with BE and LDT measurements: The applied shear strain rate was 0.1 %/min and it was draining from both ends. Additionally, local strain measurements were done in this series by using LDTs set axially and diametrically. Shear wave velocity of medium these dense specimens (Dr≈70%) was also measured by using bender elements set at both ends and shear modulus was calculated.

Series III) CD tests: Specimens were drained from both ends, very similar to Series II tests. A constant strain rate of 0.1 %/min, as recommended in JGS 0524 (2009), was applied for shearing the dense (Dr≈80%) test specimens in this series.

4. TEST RESULTS

(1) Difference between local and external axial strain

As discussed in Section 3.2, local axial strains were measured by two LDTs (LDT1 and LDT2) in longitudinal direction by attaching them directly to the specimen membrane (see Fig. 2) in Series II tests. The external axial strain ($\varepsilon_{a,\mathrm{ext}}$) was also measured with LVDT placed outside the triaxial cell. As a representative plot, local axial strain values from LDT1 ($\varepsilon_{a,\mathrm{LDT1}}$) and LDT2 ($\varepsilon_{a,\mathrm{LDT2}}$) plotted against the stress-ratio under confining stresses of 100 kPa and 400 kPa are shown in Fig. 3a and 3b respectively. The average local axial strain ($\varepsilon_{a,\mathrm{LDT\ ave}}$) is obtained by averaging $\varepsilon_{a,\mathrm{LDT1}}$ and $\varepsilon_{a,\mathrm{LDT2}}$.

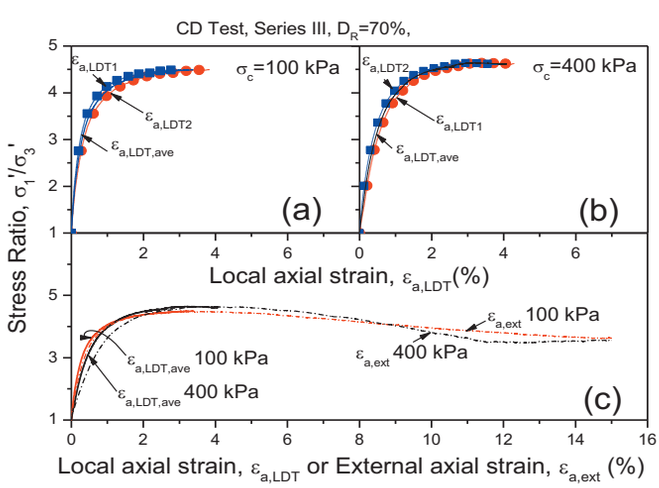

Fig. 3 Individual data for local axial strain ($\varepsilon_{a,LDT1}, \varepsilon_{a,LDT2}$) at a) σ_c'=100kPa and b) σ_c'=400kPa, and c) comparative view of average local axial strain ($\varepsilon_{a,\mathrm{LDT\ ave}}$) obtained in Figs 6a and 6b against an external axial strain for Series III tests under confining stress (σ_c') =100kPa and 400kPa.

Fig. 3c shows a comparative view of stress-ratio variation against an external axial strain ($\varepsilon_{a,\mathrm{ext}}$) and average local axial strains ($\varepsilon_{a,\mathrm{LDT\ ave}}$). For the same stress ratio, external axial strains at both confining stresses are slightly larger than the local strains implying that $\varepsilon_{a,\mathrm{ext}}$ includes some localized deformation at specimen ends, also called as bedding error. The very small difference however signifies that the error in axial measurement for Series I and III, where local strain measurement was not done, is not much appreciable.

(2) Stress-strain behavior

Consolidated undrained ($\overline{CU}$) triaxial tests

Results of Series I $\overline{CU}$ test conducted at three different confining pressures are shown in Fig. 4. In the plots, stress ratio $(= \sigma_1'/\sigma_3')$ and pore water pressure are plotted against the external axial strain ($\varepsilon_{a,\text{ext}}$) obtained from the LVDT placed outside the triaxial cell. The stress ratio curves at various confining stresses are almost overlapping that confirms the reproducibility of test specimens and test conditions. Strain-softening behavior in the post-peak region for this series (Fig. 4a) is relatively mild. The pore water pressure versus $\varepsilon_{a,\text{ext}}$ curves (Fig. 4a, right vertical axis) show that positive pore water pressure builds up during initial loading but then drops to a negative value showing a highly dilatant nature of the sand. The general trend is that the positive pore water pressure built-up is higher for higher confining condition but attain almost similar negative pressure level at the latter part of shearing. It is noted here that the negative pore water pressure built-up that measured as low as -74kPa could not be stopped even by applying significantly large back pressure of 200 kPa. Fig. 4b presents the deviator stress (q) vs. mean effective stress (p') relation for the tests in Series I. In order to draw the critical state line (CSL) defined by Eq. 3 below, that corresponds to steady state failure state (hereafter used the terminology, 'failure line' or 'at failure'), the q-p' values at residual stage ($\varepsilon_{a,\text{ext}}$≈15%) are considered. The CSL corresponding to the peak stress state is also drawn. The overall trend of CSL at peak stress and at failure are shown by the solid and dash-dot lines, respectively.

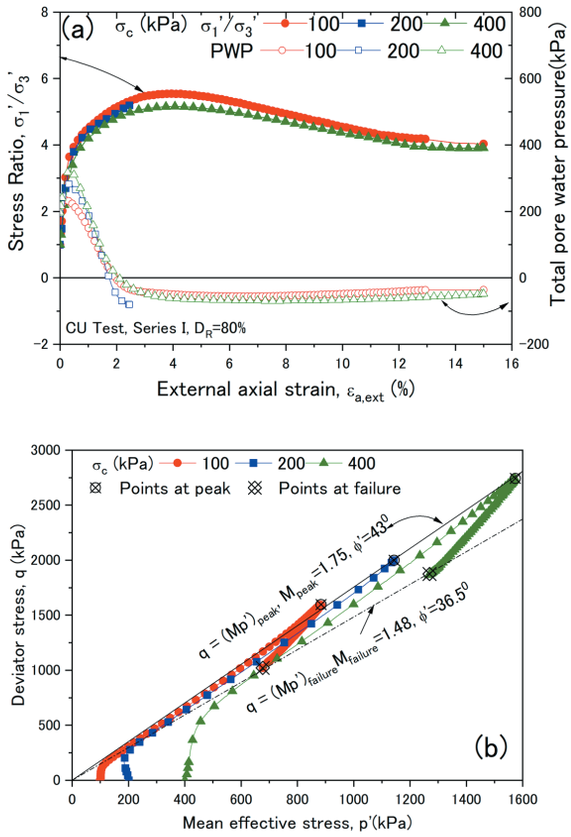

Fig. 4. Relationships showing; a) stress ratio and pore water pressure vs. axial strain, and b) q-p' plots for Series I $\overline{CU}$ test.

$$q = Mp' \quad \text{(Eq. 3)}$$

$$\sin \emptyset' = 3M/(6 + M) \quad \text{(Eq. 4)}$$

where, $\emptyset'$ =friction angle, q: deviator stress $= (\sigma_1' - \sigma_3')$, p': mean effective stress$= (\sigma_1' + 2\sigma_3')/3$ and M: critical state parameter defined as the slope of q-p' line corresponding to the peak or failure states.

The friction angle ($\emptyset'$) based on Eq. 4 at failure for this series is 36^0, but tends to become as high as 43^0 at peak stress state.

Drained triaxial compression (CD) tests

In addition to $\overline{CU}$ test mentioned above, two CD test Series (Series II and III) were conducted to obtain more understanding on the strength characteristics of Albany silica sand. The stress-strain variation (q-$\varepsilon_{a,\text{ext}}$) and volumetric strain measured by a burette ($\varepsilon_{\text{vol, meas}}$) -$\varepsilon_{a,\text{ext}}$ plots for Series II and Series III tests are shown in Figs. 5a and 5c respectively. Apparent peak stress points, significant volumetric dilation and continuous strain-softening behavior could be observed. Comparatively larger strain-softening in Fig. 5c can be related to the higher relative density of Series III test specimens.

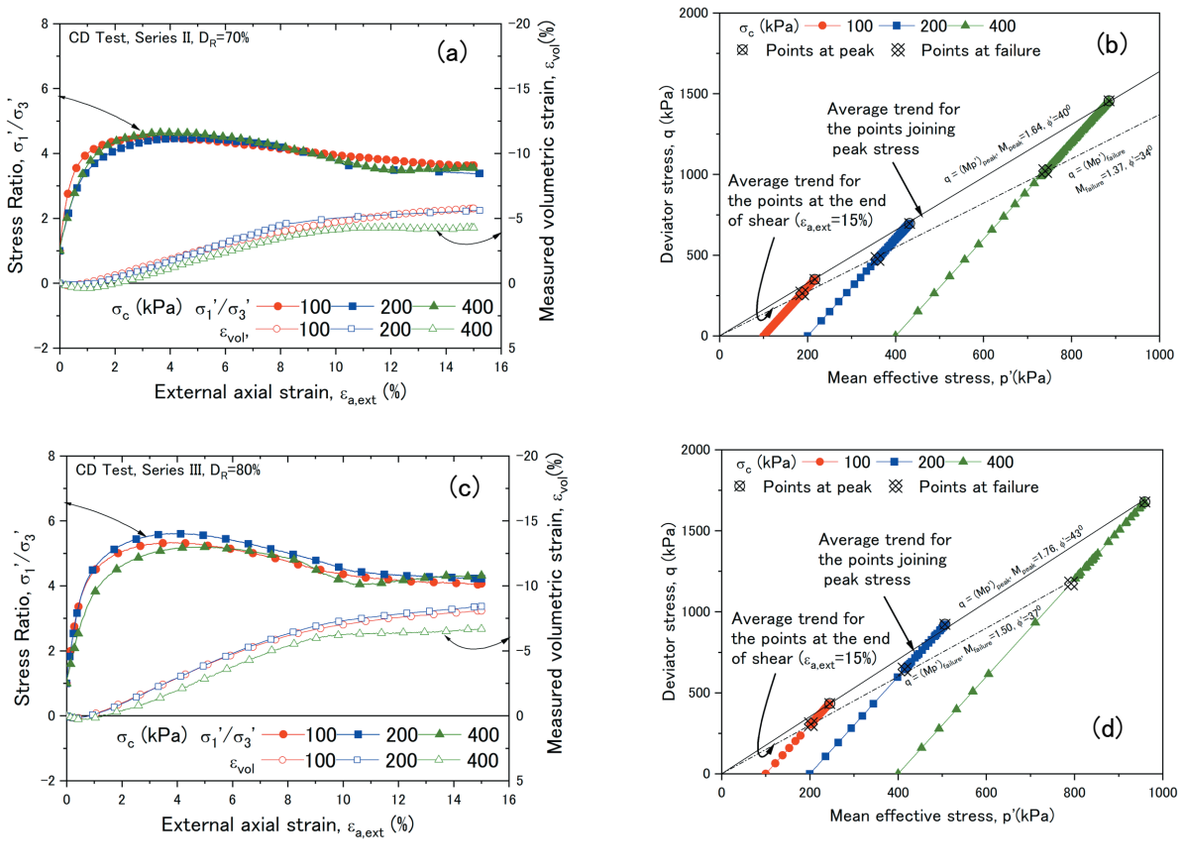

Fig. 5. Relationships showing; a, c) stress ratio and pore water pressure vs. axial strain, and b,d) q-p' plots for Series II and Series III CD test respectively

The three parallel lines with markers in Fig. 5b show the q-p' relations for the drained triaxial test data in Series II and those in Fig. 5d, represent Series III. Based on the points of peak stress in these three tests, the average trend is shown by a solid line in each plot. On the other hand, the dotted line is obtained from the q-p' values at failure ($\varepsilon_{a,\text{ext}}$≈15%). The friction angles, $\emptyset'$ for Series II tests calculated by using Eq. 4 are 40 degree for the peak stress and 34 degree at failure; whereas, it is 43 degree for the peak stress and 37 degree at failure for Series III tests. Higher friction angles at both peak and steady state failure could be interlinked to the higher relative density of Series III test specimens.

(3) Assessment of model parameters

Shear modulus from triaxial tests

The calculated Secant Young's modulus at 0.01% strain level ($E_{sec,0.01}$), the ratio of the deviator stress and 0.01% external axial strain, are summarized in Table 2. In the table, shear modulus at corresponding strain level, $G_{sec,0.01}$ are derived from $E_{sec,0.01}$ by using Eq. 5 and assuming Poisson's ratio, ν as 0.3 for drained tests and 0.5 for undrained tests. Values in the parenthesis are relatively higher and were obtained from the strain measured by LDT ($\varepsilon_{a,LDT,ave}$) in Series II tests that excludes bedding error.

$$G_{sec,0.01} = \frac{E_{sec,0.01}}{2(1+\nu)} \quad \text{(Eq. 5)}$$

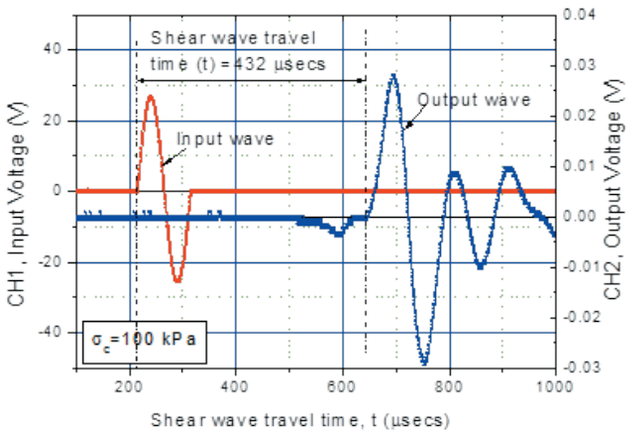

Fig. 6. A typical bender element trace under confining pressure of 100kPa showing an input and received shear wave traces.

Table 2. Shear moduli calculated from stress-strain relationship

Series	Confining stress σ_c' (kPa)	Initial void ratio e	$E_{sec,0.01}$ (MPa)	$G_{sec,0.01}$ (MPa)
I	100	0.551	118.6	39.5
CŪ tests	200	0.529	170.0	56.7
(Dr = 80%)	400	0.541	432.0	144.0
II	100	0.590	122.2 (153.9)	47.0 (59.2)
CD tests[1)]	200	0.582	115.0 (234.1)	44.2 (90.0)
(Dr = 70%)	400	0.578	344.0 (320.6)	132.3 (123.3)
III	100	0.541	122.0	46.9
CD tests	200	0.546	303.0	116.5
(Dr = 80%)	400	0.551	350.0	134.6

1) For Series II, $E_{sec,0.01}$ values were calculated from LDT (in parentheses) and LVDT records. For other series, $E_{sec,0.01}$ values were determined from LVDT only.

Shear modulus from shear wave velocity

Record traces of the bender element signal for shear wave velocity measurement under confining pressure of 100kPa just before shearing in Series II tests are shown in Fig. 6 as an example. The sinusoidal input wave generated by function generator was amplified to about ±25V before applying to the transmitter bender (CH1). The start-to-start method (Lohani et. al., 1999; JGS-TC29, 2005) for reading the arrival wave was employed to get the shear wave travel time within the specimen. In calculating the velocity, the distance

between the tip-to-tip of the top and bottom benders defined in above references was considered as the travel length. The shear wave velocity and shear modulus calculated at the start of shearing corresponding to each confining stress are summarized in Table 3. Eq. 6 was used for calculating shear moduli from the bender element tests ($G_{f,BE}$) in the table.

$$G_{f,BE} = \rho_t {V_s}^2 \quad \text{(Eq. 6)}$$

where, ρ_t: wet density of soil calculated from the known void ratio and specific gravity and V_s: shear wave velocity.

Table 3. Shear moduli calculated from shear wave velocity measured by bender elements

Series	Confining stress σ_c' (kPa)	Wet density, ρ_t (g/cm^3)	Length (mm)	Time (μs)	S-wave velocity V_s (m/s)	$G_{f,BE}$ (MPa)
II CD tests (Dr = 70%)	100	2.039	87.811	432	203.3	84.3
	200	2.044	89.096	268	332.4	225.9
	400	2.047	88.480	257	344.3	242.6

Correlation of obtained modulus with other sands

Results in this study were compared with the Toyoura sand data obtained from resonant column tests (Iwasaki and Tatsuoka, 1977) (Fig. 7). In order to compensate the void ratio (e) difference, the stiffness data were normalized with a void ratio function, $f(e)$, given by Eq. 7 originally proposed by Hardin and Richart (1963).

$$f(e) = \frac{(2.17 - e)^2}{(1 + e)} \quad \text{(Eq. 7)}$$

BE test data and a fitting curve, indicated by a dashed line, shows a closer variation with Toyoura sand data but a little larger mean effective stress exponent. The stiffness data obtained from triaxial tests are also plotted together in the same figure and are significantly smaller than those of the bender element measurements. The difference of stiffness is probably attributed due to rather larger strain considered for stiffness evaluation in triaxial compression tests as compared to 0.001% or smaller in bender element tests. It is quite tough to determine shear moduli at very small strain level from triaxial tests without local strain measurement therefore, bender element method is one of the most viable approaches to evaluate them with higher accuracy.

Friction angle

Friction angles obtained from for CD tests in Fig. 5 are summarized in Table 4. The friction angles at failure, ϕ_{f}' or $\phi_{\mathrm{d,f}}$ are within a narrow range from 34 to 37 degrees irrespective of the relative density,

drained condition and confining stress. On the contrary, the friction angles at peak stress, ϕ'_{pk} or $\phi_{d,pk}$ vary from 36 to 43 degrees, depending on the relative density of the sand. Figure 8 shows the results of current series on Albany sand compared with the data from above reference Fukushima and Tatsuoka, (1984). It is understood that there is sufficient resemblance in frictional characteristics between these two sands, although having different maximum and minimum void ratio values.

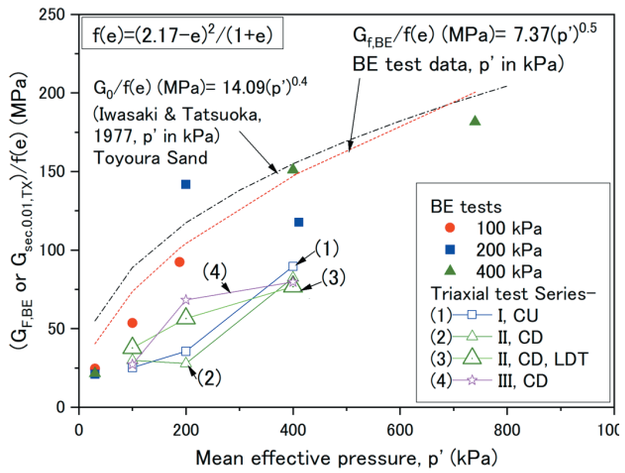

Fig. 7. Comparison of shear modulus data obtained from bender element and triaxial tests for Albany sand along with Toyoura sand data from Iwasaki and Tatsuoka (1977).

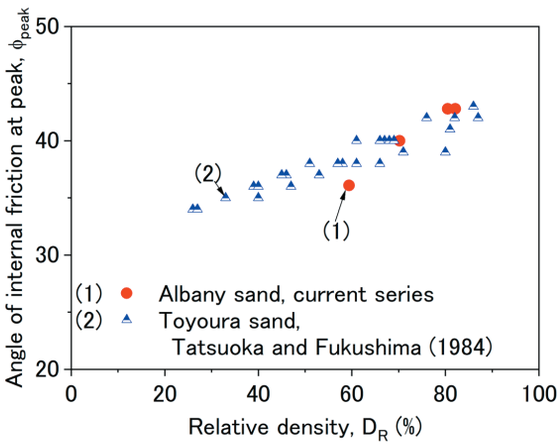

Fig. 8. Angle of friction versus relative density results of current series plotted along with the plot from Fukushima and Tatsuoka, (1984).

Table 4. Summary of friction angles and dilatancy parameters

Test Series	Friction angles		Critical state parameters	
	ϕ'_{pk} or $\phi_{d,pk}$	ϕ'_f or $\phi_{d,f}$	M_{pk}	M_f
I CŪ tests (Dr = 80%)	43	36	1.75	1.48
II CD tests (Dr = 70%)	40	34	1.64	1.37
III CD tests (Dr= 80%)	43	37	1.76	1.50

5. CONCLUSIONS

The following conclusions were drawn for Albany sand from the above discussions.

Recording of axial strain was done by using local deformation transducers (LDTs) along longitudinal direction in one test series. Although the strains recorded by externally placed LVDT were slightly higher than those from LDTs due to the bedding error in the former one, the error was not much appreciable and the use of LDT is recommended when possible. It is therefore, assumed that external LVDT data and volume measurements used in other test series did not introduce significant error in the interpretations of test results.

Friction angles, ϕ (ϕ' and ϕ_d obtained from undrained and drained shear tests, respectively) corresponding to the peak and steady state failure condition for three different relative density states of tested samples were obtained and pretty good correlation was observed. Further verification tests are however, needed for extrapolating to very large or very small relative density.

The maximum initial shear modulus (G_{max}) evaluated from bender element (BE) tests were considerably larger than those from the triaxial tests. The difference may be attributed to the rather larger strain level (about 0.01%) considered for stiffness evaluation in triaxial compression tests as compared to the BE tests at 0.001% or smaller. While applying slower rate of loading and evaluating the stiffness at very small strain by using LDTs in triaxial testing could enable to get the closer values, BE tests are better preferred to obtain G_{max} of soil. Furthermore, the G_{max} from BE tests were in the narrow range with the Toyoura sand stiffness evaluated by Resonant column test thereby showing some similarity in these sand types.

ACKNOWLEDGEMENTS

This research was conducted as a part of joint research program between Kobe University and National Research Institute for Earth Science and Disaster Resilience. Cooperation from staffs providing direct or indirect supports are highly appreciated.

REFERENCES

Cubrinovski, M. and Ishihara, K. (2002). Maximum and minimum void ratio characteristics of sands. Soils and Foundations, Vol. 42, No.6, pp. 65-78.

Fukushima, S. and Tatsuoka, F. (1984). Strength and deformation characteristics of saturated sand at extremely low pressures. Soils and Foundations, Vol. 24, No. 4, pp. 30-48.

Goto, S., Tatsuoka, F., Shibuya, S., Kim, Y. S., and Sato, T. (1991): A simple gauge for local small strain measurement in the laboratory. Soils and Foundations, Vol. 31, No. 1, pp. 169-180.

Hardin B.O. and Richart F.E. (1963). Elastic wave velocities in granular soils. Journal of ASCE, Vol. 89, pp. 33-65.

Kawamata, Y., Nakayama, M., Towhata, I., and Yasuda, S., (2016). Dynamic behavior of underground structures in E-Defense shaking experiments, Soil Dynamics and Earthquake Eng. 82, pp. 24–39.

Iwasaki T. and Tatsuoka F. (1977). Effect of grain size and grading on dynamic shear modulus of sands. Soils and Foundations, Vol. 17. No. 3, pp. 19-35.

JGS-0523, 0524, 2534 (2009). Japanese standards and explanations of laboratory test of geomaterials. Japanese Geotechnical Society publication.

JGS-TC29 (2005). Report of the 'International parallel test on the measurement of G_{max} using bender elements' organized by TC-29.

Lohani, T. N., Imai, G., and Shibuya, S. (1999). Determination of shear wave velocity in bender element test, Proceedings of the 2nd International conference on earthquake Geotechnical Engineering, Seco e Pinto (ed.) Balkema, pp. 101-106.

MEXT and NIED (2006). Annual Report of the fiscal year 2005, Research Theme No.2, Special project for earthquake disaster mitigation in urban areas, Ministry of Education, Culture, Sports, Science and Technology and National Research Institute for Earth Science and Disaster Prevention.

MEXT and NIED (2007). Annual Report of the fiscal year 2006, Research Theme No.2 Special project for earthquake disaster mitigation in urban areas, Ministry of Education, Culture, Sports, Science and Technology and National Research Institute for Earth Science and Disaster Prevention.

Authors: 1) Senior Technical Staff and Researcher, Research Center for Urban Safety and Security (RCUSS), Kobe University, 2) Senior Researcher National Research Institute for Earth Science and Disaster Resilience, 3) Professor, Tokyo University of Marine Science and Technology, 4) Professor, RCUSS, Kobe University, 5) Professor, Kindai University